Séminaire Poincaré IX (2006) 1 – 40 Séminaire Poincaré

Chaos in Microwave resonators

Hans-Jürgen Stöckmann
Fachbereich Physik der Philipps-Universität Marburg
Renthof 5
D-35032 Marburg, Germany

1 Introduction

Up to about 1990 the quantum mechanics of classically chaotic systems, shortly termed 'quantum chaos', was essentially a domain of theory [1]. Only two classes of experimental result had been available at that time. First, there were the spectra of compound nuclei giving rise to the development of random matrix theory in the sixties of the last century, and second the experiments with highly excited hydrogen and alkali atoms in strong magnetic or strong radio frequency fields. The situation changed with the appearance of the various types of billiard experiments. After the first microwave study performed in the author's group [2] there were numerous experiments with classical waves on liquid surfaces, in plates, solids, and rods, with electrons in quantum dots, tunnelling barriers and quantum corrals, and with ultra-cold atoms confined in billiards formed by light walls. References and a more detailed account on the subject may be found in Ref. [3]. It will become clear in the following that the difference between classical waves and matter waves is not of relevance, since the universal features we shall discuss are common to all types of wave not necessarily quantum mechanically in origin. This is why 'wave chaos' would be a better term to describe this field of research, and there are authors avoiding the term 'quantum chaos' as a whole.

This article is organized as follows. After a short introduction into the subject in Section 2, concentrating on the inherent difficulties with the definition of chaos in quantum mechanics, in Section 3 the microwave technique is introduced. In the subsequent three sections various aspects of quantum chaos are presented and illustrated by experimental results. The selection was exclusively guided by the intension to provide experimental illustrations of essential theoretical results. There was not the intent to give an exhaustive overview on the subject. In Section 4 a short introduction into the concept of random matrices is given, illustrating the remarkable observation that a mayor part of the statistical properties of the spectra of chaotic systems can be obtained already if the underlying Hamiltonian is substituted by a matrix the elements of which are chosen at random, only obeying some constraints. In Section 5 universal features of the wave functions of chaotic billiards are discussed. Here a lot of exact results can be obtained from the simple assumption that at each point in the billiard the wave function may be looked upon as a superposition of waves, with the same modulus of the wave vector, entering randomly from all directions. In Section 6, semiclassical quantum mechanics is introduced, based on the disseminating papers by M. Gutzwiller, establishing a link between the quantum-mechanical Green function and the classical trajectories. The article ends with a presentation of recent applications of wave-chaos research.

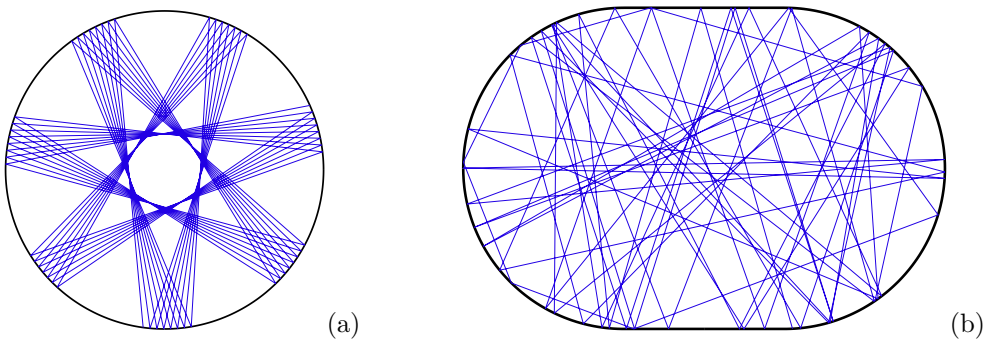

(a) (b)

FIGURE 1 – Classical trajectories in a circular (a) and a stadium (b) billiard.

2 From classical to quantum mechanics

To illustrate the difficulties one is facing with the concept of chaos in quantum mechanics, let us first consider an idealised billiard system, i. e. the classical dynamics of a single particle travelling frictionless through a box with infinitely high walls. For a circular billiard the trajectory is regular (see Fig. 1(a)). There are two constants of motion, the total energy E, and the angular momentum L. Since there are two degrees of freedom as well, the system is integrable. Small uncertainties in the initial conditions, such as the distance between two neighbouring trajectories, will therefore increase only linearly in time. The situation is qualitatively different for the stadium billiard, the guinea pig in billiard research (see Fig. 1(b)). There is only one constant of motion left, the total energy E, and the distance between neighbouring trajectories increases exponentially with time. The stadium billiard thus is chaotic.

In quantum mechanics this distinction between integrable and chaotic systems does not work. The initial conditions are defined only within the limits of the uncertainty relation

$$\Delta x \, \Delta p \leq \frac{1}{2}\hbar \,, \tag{1}$$

and the concept of trajectories looses its significance. One may even ask whether quantum chaos does exist at all. Since the Schrödinger equation is linear, a quantum mechanical wave packet can be constructed from the eigenfunctions by the superposition principle. But if the wave packet once has been generated, its evolution for arbitrarily long times is available without any problem. There is no room left for chaos.

On the other hand the correspondence principle demands that there *must* be a relation between *linear* quantum mechanics and *nonlinear* classical mechanics at least in the regime of large quantum numbers. This apparent contradiction has been resolved by semiclassical quantum mechanics, derived in essential parts by M. Gutzwiller in a series of papers (see Ref. [4] for a review). The theory relates classical trajectories to quantum mechanical spectra and wave functions, and this defines the program of quantum chaos research, namely to look for the fingerprints of classical chaos in the quantum mechanical properties of the system.

Billiards are ideally suited systems for this purpose. The numerical calculation of the classical trajectories is elementary, and the stationary Schrödinger equation reduces to a simple wave equation

$$-\frac{\hbar^2}{2m}\left(\frac{\partial^2}{\partial x^2}+\frac{\partial^2}{\partial y^2}\right)\psi_n = E_n\psi_n \,. \tag{2}$$

The potential appears only in the boundary condition $\psi_n|_S = 0$, where S is

the surface of the billiard. Though billiard systems are conceptually simple, they nevertheless show the full complexity of non-linear systems.

A further advantage is the equivalence of the stationary Schrödinger equation with the time-independent wave equation, the Helmholtz equation

$$-\left(\frac{\partial^2}{\partial x^2}+\frac{\partial^2}{\partial y^2}\right)\psi_n = k_n^2\psi_n\,, \tag{3}$$

where ψ_n now is the amplitude of the wave field.

FIGURE 2 – Chladni giving a public demonstration of his sound figures.

The equivalence of the stationary Schrödinger equation and the Helmholtz equation opens the opportunity to study questions and to test theories, originally motivated by quantum mechanics, by means of classical waves. The boundary conditions for the classical and the corresponding quantum mechanical systems may differ, but this is not of relevance for the questions to be treated in this article.

The first experiment of this type dates back already more then 200 years. At the end of the 18th century E. Chladni developed a technique "to make sound visible", by decorating the nodal lines of vibrating plates with grains of sand. Chladni never achieved to get a permanent position at an university and earned his livings by giving demonstrations of his experiments to the public [5]. Figure 2 gives an example. On occasion of a stay in Paris 1808, he got an invitation by Napoleon to give a private performance in the Tuileries [6]. There is a very vivid report by Chladni on this visit [7] :

"When I entered, he welcomed me, standing in the centre of the room, with the expressions of his favour. Napoleon showed much interest in my experiments and explanations and asked me, as an expert in mathematical questions, to explain all topics thoroughly, so that I could not take the matter too easy. He was well informed that one is not yet able to apply a calculation to irregularly shaped areas, and that, if one were successful in this respect, it could be useful for applications to other subjects as well."

The last remark had been really visionary ! Who could have imagined at that time that Chladni's experiments in a sense mean the starting point of quantum chaos research ?

3 Microwave billiards

Modern experimental billiard studies started with microwave resonators [2]. Fig. 3(left) shows a typical set-up. The cavity is formed by a bottom plate supporting the entrance antenna, and by an upper part whose position can be moved with respect to the lower one. As long as a maximum frequency $\nu_{max} = c/2d$ is not exceeded, where d is the height of the resonator and c the velocity of light, the system can be considered as quasi-two-dimensional. In this situation the electro-magnetic wave equations reduce to the scalar Helmholtz equation (3), where ψ_n corresponds to the electric field pointing perpendicularly from the bottom to the top plate. Since the electric field component parallel to the wall must vanish, we have the condition $\psi_n|_S = 0$ on the outer circumference S of the resonator. We have thus arrived at a complete equivalence between a two-dimensional quantum billiard and the corresponding quasi-two-dimensional microwave resonator, including the boundary conditions. As an example Fig. 3(right) shows the reflection spectrum of a microwave resonator of the shape of a quarter stadium [2]. Each minimum in the reflection corresponds to an eigenfrequency of the resonator.

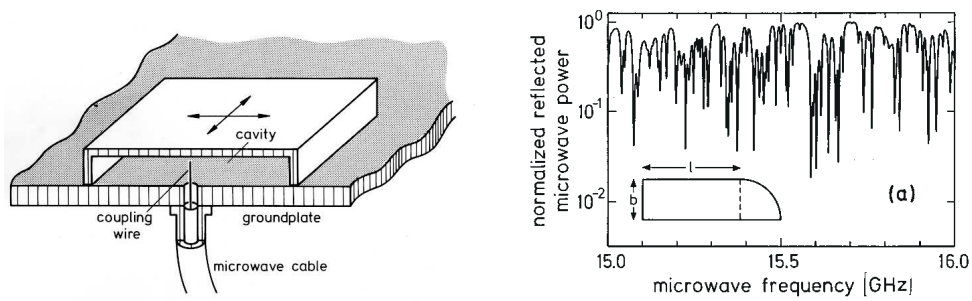

FIGURE 3 – Microwave set-up to study spectra and wave functions (left), and a typical microwave reflection spectrum (right) [2].

A detailed consideration shows that the measurement directly yields the components of the scattering matrix S, where the diagonal element S_{nn} corresponds to the reflection amplitude at the nth antenna, and the off-diagonal matrix element S_{nm} to the transmission amplitude between antennas n and m. For isolated resonances the components of the scattering matrix are given by

$$S_{ij}(\vec{r}_i, \vec{r}_j, k) = \delta_{ij} - 2\imath\gamma \sum_n \frac{\bar{\psi}_n^*(\vec{r}_i)\bar{\psi}_n(\vec{r}_j)}{k^2 - \bar{k}_n^2 + \imath\Gamma_n}\,, \tag{4}$$

where $\bar{k}_n$ and $\bar{\psi}_n(\vec{r}_i)$ are the nth k-eigenvalue and eigenfunction at the position of antenna i. The bar denotes that both quantities are slightly changed as compared

to the closed system. γ is a factor describing the antenna coupling, assumed to be equal for all antennas for the sake of simplicity. In addition the resonances acquire a line width Γ_n. Apart from these modifications the microwave measurement yields directly the Green function of the system, and thus the complete quantum mechanical information. Eq. (4) is the quantum-mechanical expression of the scattering matrix. The electromagnetical line widths γ_n are related to the Γ_n by $\Gamma_n = k\gamma_n$ [8]. This is a consequence of the different dispersion relations $\omega \sim k$ and $\omega \sim k^2$ for the electromagnetic and the quantum-mechanical case, respectively.

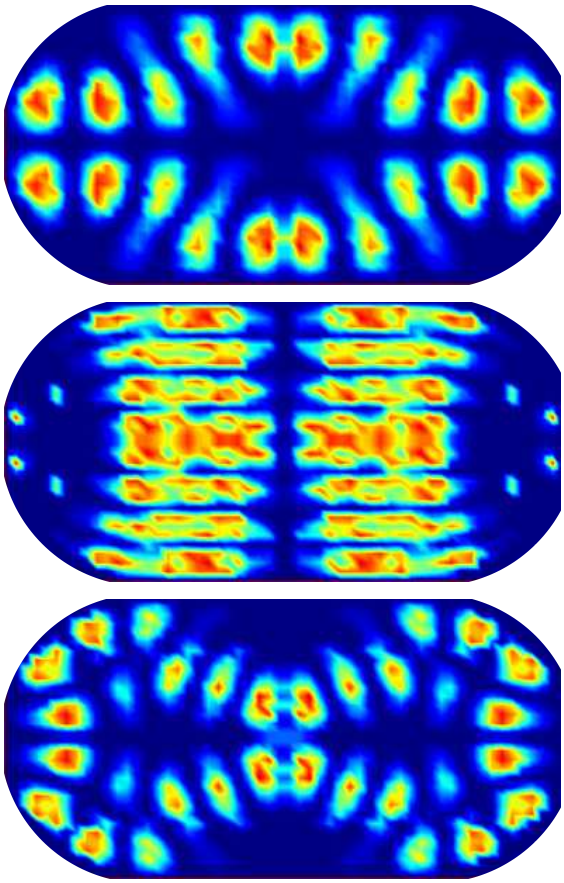

FIGURE 4 – Wave functions in a stadium-shaped microwave resonator [9]. The figure shows $|\psi_n(r)|^2$ in a colour plot.

Equation (4) shows that the depth of a resonance contains the information on the wave functions $\psi_n(r)$ at the antenna positions. By scanning with the antenna through the billiard $\psi_n(r)$ may thus be spatially resolved. Figure 4 shows a number stadium wave functions obtained in this way [9]. All wave functions show the phenomenon of scarring, meaning that the wave function amplitudes are not distributed more or less homogeneously over the area, but concentrate along classical periodic orbits. The phenomenon had been first described and termed by E. Heller [10]. The figure could give the impression that scarred wave functions are dominating, but this is only true for the lowest eigenvalues. With increasing energy the fraction of scarred wave functions tends to zero.

From the Fourier transform of the Green function the propagator is obtained, either the electro-magnetic or quantum-mechanical one, depending on the used dispersion relation [11]. Thus also the study of pulse propagation becomes possible.

Microwave billiards have a number of advantages as compared to nuclei : (a) typical wave lengths are of the order of mm to cm, resulting in very convenient sizes for the used resonators, (b) shapes of the resonators, coupling strengths to antennas etc. can be perfectly controlled, (c) parameter variations, e. g. of the coupling strength, the position of an impurity, or of one length can be easily achieved, and (d) last but not least, we have seen that in microwave systems the complete scattering matrix is obtainable, including the phases. This is extraordinary, in standard scattering experiments, such as in in nuclear physics, usually only reduced information, such as scattering cross-sections, is available, resulting in a complete loss of the phase information. This is why a number of predictions of scattering theory have been tested not in nuclei but microwave billiards.

4 Random Matrices

In the spring times of nuclear physics in the midst of the last century there appeared a vast amount of experimental results on cross-sections, partial cross-section etc., obtained by bombarding target nuclei with light projectiles. Nearly nothing was known at that time on the origin of the nuclear forces. Could it be expected under such circumstances to obtain any relevant information at all from these irregularly looking spectra without any recognisable pattern ? Here one idea showed up to be extremely useful, notwithstanding its obviously oversimplifying nature : If nothing is known on the nuclear Hamiltonian H, just let us take its matrix elements in some basis as random numbers, with only some global constraints, e. g. by taking the matrix H symmetric for systems with, or Hermitian for systems without time-reversal symmetry, and by fixing the variance of its matrix elements. Assuming basis invariance of the distribution of the matrix elements one immediately sees that the matrix elements are uncorrelated and Gaussian distributed [12]. There are three Gaussian ensembles, the orthogonal one (GOE) for time-reversal invariant systems with integer spin, the unitary one (GUE) for systems with broken time-reversal symmetry, and the symplectic one (GSE) for time-reversal invariant systems with half-integer spin. Here 'orthogonal' etc. refers to the invariance properties of the respective ensembles. Recently it has been shown by M. Zirnhauer [13] that in fact there are seven additional ensembles, which become relevant, whenever pair-wise creation and annihilation of particles is involved, as it is the case in elementary particle physics and superconductivity. For all Gaussian ensembles exact expressions for many quantities of interest can be calculated explicitly, such as spectral correlation functions, eigenvalue spacings distributions etc. .

The quantity most often studied in this context is the distribution of level spacings $p(s)$ normalised to a mean level spacing of one. For 2×2 matrices this quantity can be easily calculated, yielding for the GOE the famous Wigner surmise

$$p(s) = \frac{\pi}{2} s \exp\left(-\frac{\pi}{4} s^2\right) . \tag{5}$$

For large matrices Eq. (5) is still a good approximation with errors on the percent level. Fig. 5 shows level spacings distributions for a variety of chaotic systems, all showing the same behaviour. Such observations had been the motivation for Bohigas, Giannoni and Schmitt [14] to formulate, what is today known as the BGS conjecture : *"Spectra of time-reversal-invariant systems whose classical analogs are K systems show the same fluctuation properties as predicted by GOE (alternative stronger conjectures that cannot be excluded would apply to less chaotic systems, provided that they are ergodic). If the conjecture happens to be true, it will then have been established the* universality of the laws of level fluctuations *in quantal spectra already found in nuclei and to a lesser extent in atoms. Then, they should also be found in other quantal systems, such as molecules, hadrons, etc."*. The paper had been extremely influential and initiated a complete program of quantum chaos research. To be

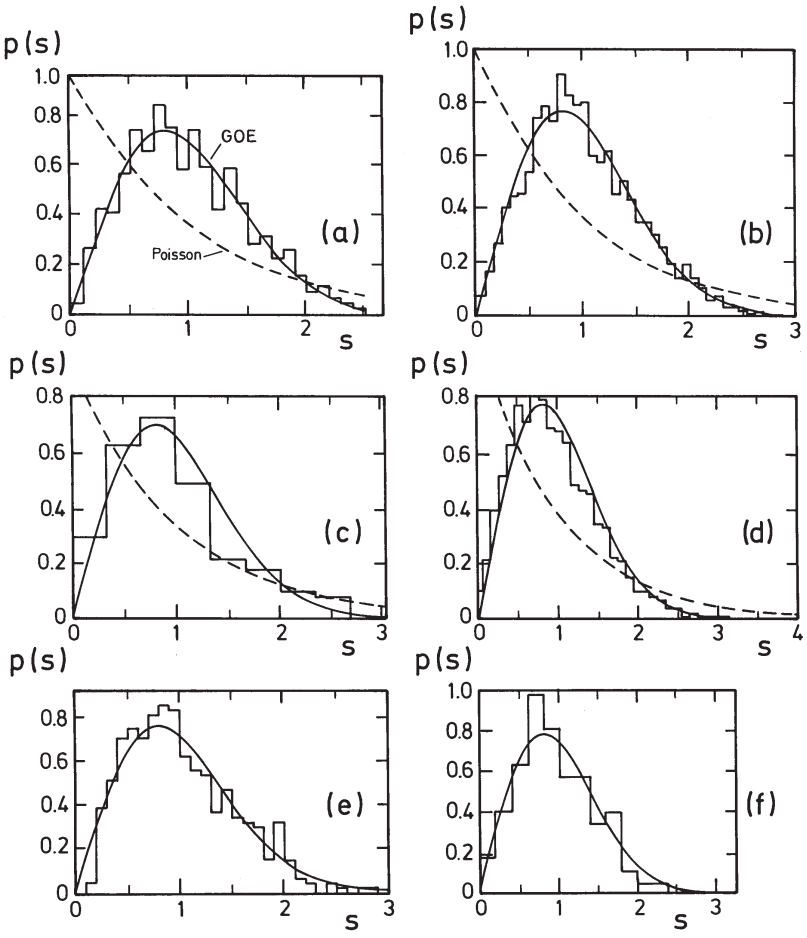

FIGURE 5 – Level spacing distribution for a Sinai billiard (a), a hydrogen atom in a strong magnetic field (b), the excitation spectrum of a NO_2 molecule (c), the acoustic resonance spectrum of a Sinai-shaped quartz block (d), the microwave spectrum of a three-dimensional chaotic cavity (e), and the vibration spectrum of a quarter-stadium shaped plate (f) (taken from Ref. [3]). In all cases a Wigner distribution is found though only in the first three cases the spectra are quantum mechanically in origin.

fair one should mention that there had been another paper on the same subject [15] somewhat earlier, which, however, at that time did not find the attendance it would have deserved.

The replacement of H by a random matrix means to abandon any hope to learn more about nuclei from the spectra but some average quantities such as the mean level spacings. Of course this is not the end of the story : there *are* techniques to extract also individual system properties. We shall come back to this aspect in Section 6. But the loss of individual features in the spectra on the other hand means that it might be worthwhile to look for *universal* features being common to all chaotic systems. This approach showed up to be extremely fruitful. It allowed to apply results originally obtained for nuclei to many other systems as well, in particular quantum-dot systems [16] and microwave billiards [3].

In addition to the level spacings distribution in particular spectral correlations

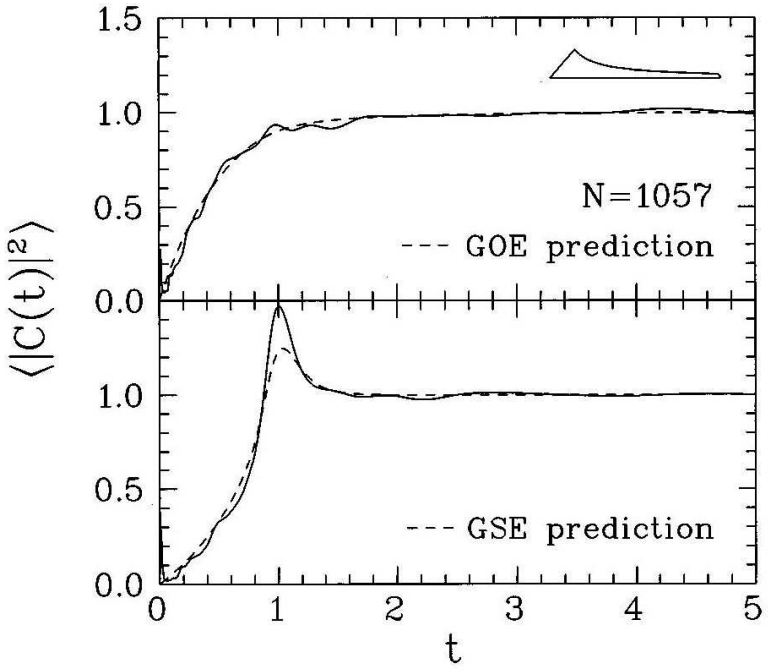

FIGURE 6 – Spectral form factor for the spectrum of a microwave hyperbola billiard (top), and for the subspectrum obtained by considering only every second resonance (bottom) [17].

related to the spectral auto-correlation function $C(E) = \langle\rho(E_2)\rho(E_1)\rangle - \langle\rho(E_2)\rangle\langle\rho(E_1)\rangle$ are considered, where $E = E_2 - E_1$, and the brackets denote a spectral average. Quantities often studied in literature are number variance and spectral rigidity, see e. g. Ref. [3] for details. Here another object shall be considered, the spectral form factor $K(t)$, since it will be of importance for the understanding of the relation between random matrix theory and semiclassical quantum mechanics to be discussed in Section 6. $K(t)$ is obtained from the Fourier transform of the spectral auto-correlation function. Random matrix theory yields explicit expressions. For later use the results for the GOE and the GUE shall be given (see e. g. Ref. [1]) :

$$K_{\rm GOE}(t) = \begin{cases} 2t - t\ln(1+2t) \\ 2 - t\ln\frac{2t+1}{2t-1} \end{cases} \quad , \qquad K_{\rm GUE}(t) = \begin{cases} t & t<1 \\ 1 & t>1 \end{cases} \quad . \tag{6}$$

The time is given in units of the Heisenberg time $t_H = \hbar/\langle\Delta E\rangle$, where $\langle\Delta E\rangle$ is the mean level spacings.

Fig. 6 shows as an experimental example the spectral form factor for a hyperbola billiard obtained in the group of A. Richter [17]. In the upper part of the figure $K(t)$ for the *complete* spectrum is shown. There is a good agreement with random matrix predictions from the GOE. This is consistent with the fact that microwave billiard systems are time-reversal invariant, and there is no spin. Spectra showing GSE statistics have not yet been studied experimentally, but there is the remarkable fact that GSE spectra can be generated by taking only every second level of a GOE spectrum [12]. Exactly this had been dome with the spectrum of the hyperbola billiard to obtain the spectral form factor in the lower part of the figure, being in perfect agreement with the expected GSE behaviour.

5 The random plane wave approximation

In a disseminating paper on wave functions in the stadium billiard McDonald and Kaufman noticed [18] that for most wave functions the amplitudes ψ are Gaussian distributed,

$$P_\psi(\psi) = \sqrt{\frac{A}{2\pi}} \exp\left(-\frac{A\psi^2}{2}\right) , \tag{7}$$

where A is the billiard area. Exceptions are scarred wave functions of the type shown in Fig. 4. For the intensities $\rho = |\psi|^2$ of the wave function follows a Porter-Thomas distribution,

$$P_\rho(\rho) = \sqrt{\frac{A}{2\pi\rho}} \exp\left(-\frac{A\rho}{2}\right) . \tag{8}$$

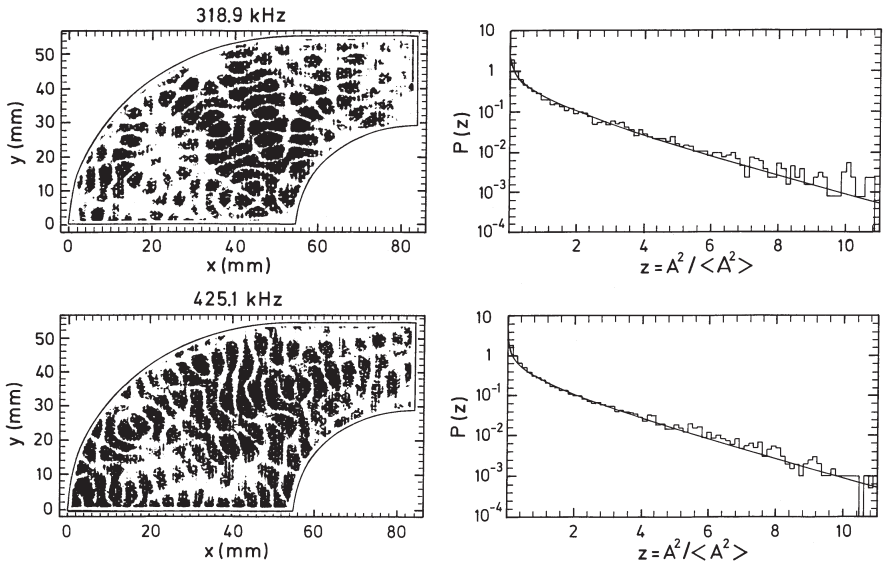

FIGURE 7 – Vibration amplitude pattern for two eigenfrequencies of a plate of a quarter Sinai-stadium billiard (left column) and corresponding distribution function for the squared amplitudes. The solid line corresponds to a Porter-Thomas distribution, see Eq. (8) [19].

This phenomenology is not restricted to quantum-mechanical systems. Figure 7 shows two vibration patterns for a plate of the shape of a quarter Sinai-stadium, together with the distribution functions for the squared amplitudes [19]. In both cases a perfect agreement with a Porter-Thomas distribution is found.

These findings can be explained under the assumption that at any point of the billiard the wave function may be considered as a superposition of plane waves [21]

$$\psi(k, \vec{r}) = \sum_n a_n e^{\imath \vec{k}_n \vec{r}} , \tag{9}$$

entering from random directions $\vec{k}_n/k$, and random amplitudes a_n, but with the modulus $k = |\vec{k}_n|$ of the wave vector fixed. The Gauss distributions of the wave function

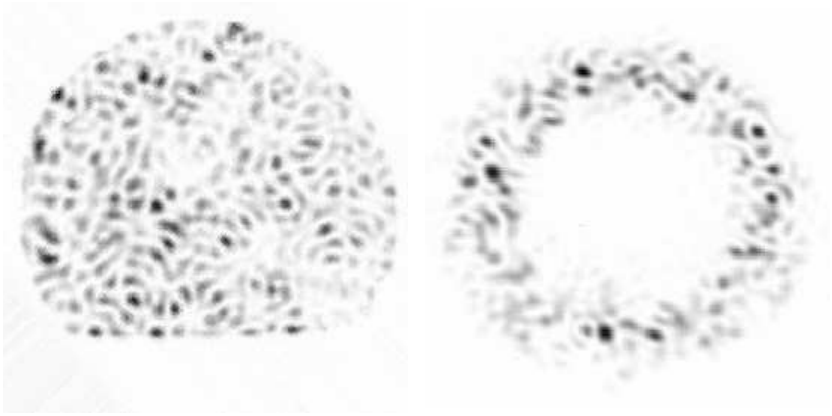

FIGURE 8 – Near-field (left) and far-field (right) emission patterns after sending laser light through a D-shaped glass fiber (diameter $d = 107\,\mu$m) [20].

amplitudes are then an immediate consequence of the central limit theorem. A more thorough foundation of the ansatz can be found in Ref. [22].

V. Doya et al. [20] succeeded in a nice demonstration of the model by sending laser light through a glass fiber with a D-shaped cross-section. The light output directly at the end of the fiber exhibits a chaotically looking speckle pattern, see Fig. 8(left). The right hand part shows the corresponding far-field pattern, obtained by just putting an additional lens into the optical path. The far-field concentrates on a ring with $|k| = \text{const.}$, thus illustrating the validity of the model.

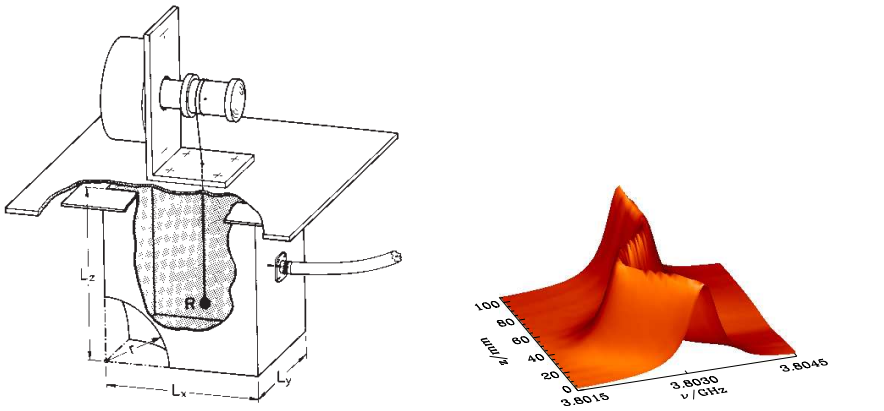

(a) (b)

FIGURE 9 – Experimental set-up to measure field distributions in a three-dimensional Sinai microwave resonator with $L_x = 96\,\text{mm}$, $L_y = 82\,\text{mm}$, $L_z = 106\,\text{mm}$, $r = 39\,\text{mm}$ (a) and frequency-shift spectrum for one resonance obtained by pulling the sphere perpendicularly through the resonator (b) [23].

It had been mentioned already that most of the concepts developed in quantum chaos research may be adopted to all types of classical waves as well. Let us take a three-dimensional microwave resonator as an example. In the general case the Maxwell equations cannot be reduced to the scalar wave equation (3) any longer, and there are altogether three boundary conditions which have to be obeyed on metallic surfaces,

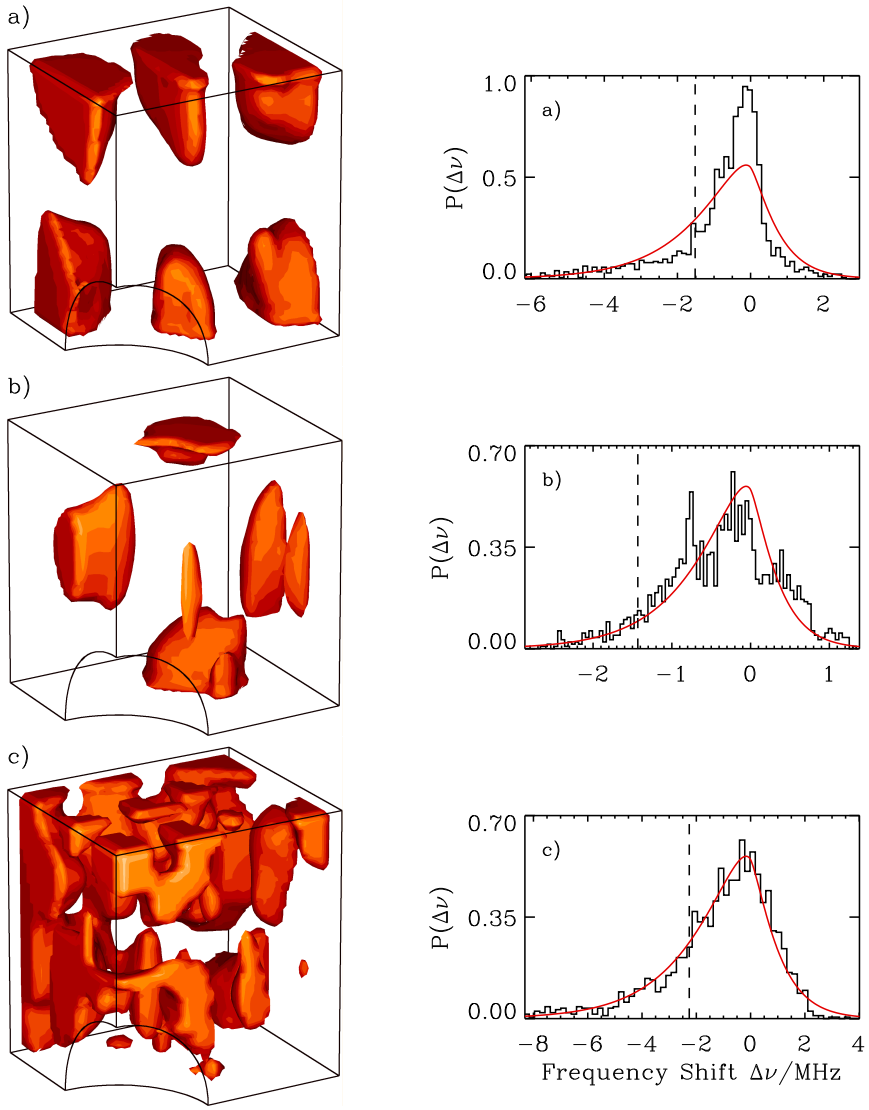

FIGURE 10 – Field distributions for three typical eigenfrequencies at $\nu = 5.208\,\mathrm{GHz}$ (a), $2.897\,\mathrm{GHz}$ (b), $8.293\,\mathrm{GHz}$ (c) for the three-dimensional Sinai resonator (left column), and corresponding frequency shift distribution (right column) [23].

namely

$$\nabla_\perp E|_S = 0\,, \qquad \nabla_\parallel B\big|_S = 0\,, \tag{10}$$

where $\nabla_\perp$, $\nabla_\parallel$ are the components of the gradient, perpendicular and parallel to the surface.

The resonator used in the experiment consisted of a rectangular box with the octant of a sphere removed from one of the corners. It is thus a three-dimensional analog of a Sinai billiard. A metallic sphere suspended at a thread could be pulled through the resonator by means of a step motor. Fig. 9 shows the experimental set-up, together with an example of a frequency shift measurement.

The fields have to adjust to the boundary conditions at the surface of the sphere, generating a frequency shift $\Delta\nu$ of the eigenfrequencies proportional to $-2\vec{E}^2 + \vec{B}^2$. Typical field distributions obtained in this way are shown in the left column of Fig. 10

[23]. To visualise the distributions, a surface of constant frequency shift, i. e. of a constant value of $-2\vec{E}^2 + \vec{B}^2$, has been shaded. The examples shown allow an easy interpretation. The field distribution in the upper panel corresponds to a standing wave between the vertical planes, whereas the field distribution shown in the central row is scarred along a periodic orbit of the shape of a diamond. Finally, the field distribution in the bottom panel has a completely chaotic appearance.

To substantiate these observations, on the right column of Fig. 10 the distributions of frequency shifts $\Delta\nu \sim -2\vec{E}^2 + \vec{B}^2$ are plotted. Under the assumption that all six field components E_x, ..., B_z are uncorrelated and Gaussian distributed, the frequency shift distribution function can be calculated. The result is the solid line. A perfect agreement with the experiment is found for the chaotically looking field distribution of Fig. 10(c), whereas for the two other examples the solid line is not able to describe the experimental findings.

What does this mean ? At first sight the assumption of uncorrelated field components seems to be very strong. After all the components of $\vec{E}$ and $\vec{B}$ are intimately linked via the Maxwell equations. But if we assume again that the chaotic field distribution can be obtained by a superposition of plane waves, now of electromagnetic waves, the correlations disappear and one ends up exactly with the applied model of uncorrelated Gaussian distributed field components. The same model which had been applied with great success to quantum billiards, thus does work equally well for electromagnetic systems.

6 Semiclassical quantum mechanics

Before quantum mechanics had been established in its present form by Heisenberg, Schrödinger and others, it had been Bohr, and later Born and Sommerfeld, who developed a technique today known as semi-classical to calculate the spectrum of atomic hydrogen. At that time Einstein [24] argued that this approach must be a dead end, since semi-classical quantisation needs invariant tori in the phase space, preventing a semi-classical quantisation for non-integrable systems. This would mean that the technique applied hitherto would work for hydrogen-like systems only, since already the second element in the periodic system, Helium, is non-integrable. This had been one of the rare cases, where Einstein was wrong, though it needed half a century until M. Gutzwiller [4] showed in a series of papers that chaotic systems, too, allow for a semi-classical quantisation.

Starting point of his approach is Feynman's path integral for the quantum-mechanical propagator

$$K(q_A, q_B, t) = \int \mathcal{D}(q) W(q) \exp\left[\frac{\imath}{\hbar}\int_0^t L(q,\dot{q})\,dt\right], \tag{11}$$

giving the probability amplitude for a particle to propagate in time t from q_A to q_B. The expression on the right hand side means in a symbolical short-hand notation an integral over all pathes, classically allowed or forbidden, from q_A to q_B, where $W(q)$ takes into account the stability of the trajectory, and $L(q,\dot{q})$ is the Lagrange function. It is remarkable that both quantities are purely classical, quantum mechanics entering only via the $1/\hbar$ in the exponential. Expression (11) is not particulary useful for an explicit calculation of the propagator, since it involves a multi-dimensional integral, but it is very well suited as a starting point for a semi-classical approach.

In the semiclassical limit the phase factors are strongly fluctuating quantities, and only terms contribute significantly, where the phase is stationary, i. e. where the condition

$$\delta \int L(q,\dot{q},t)dt = 0 \tag{12}$$

is met, where the variation is over all paths connecting q_A and q_B. But this is exactly Hamilton's principle of classical mechanics, from which the classical equations of motion can be derived. Expressed in other words : In the semi-classical limit only the classically allowed paths contribute to the path integral (11) !

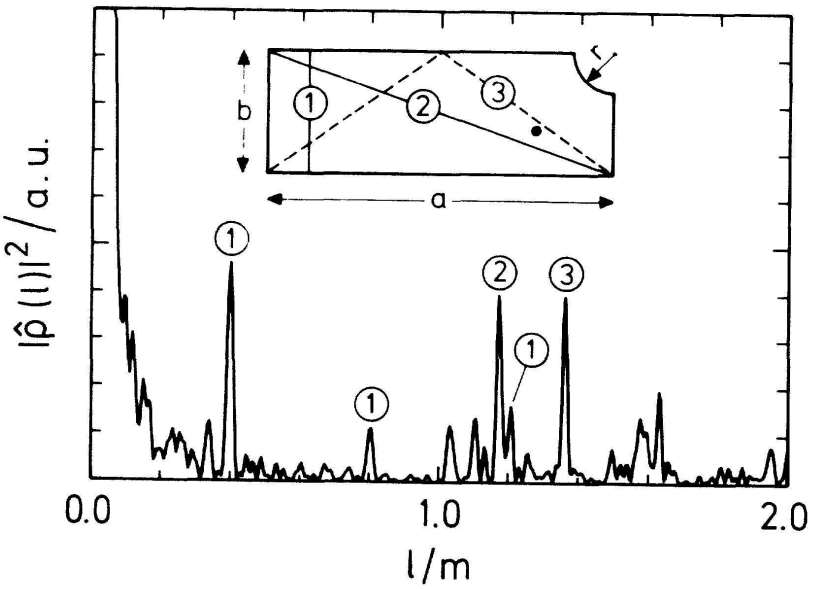

FIGURE 11 – Squared modulus $|\hat{\rho}(t)|^2$ of the Fourier transform of the spectrum of a quarter Sinai billiard ($a = 56\,\mathrm{cm}$, $b = 20\,\mathrm{cm}$, $r = 7\,\mathrm{cm}$). Each resonance can be associated with a classical periodic orbit [2].

This shall be demonstrated by two experimental examples. For the density of states Gutzwiller's approach yields his famous trace formula. It becomes particularly simple in billiard systems, if the wavenumber k is taken as the variable. In terms of k the density of states reads

$$\rho(k) = \rho_0(k) + \sum_n A_n e^{\imath k l_n} \,. \tag{13}$$

The first term varies smoothly with k and is given in its leading term by Weyl's formula

$$\rho_0(k) = \frac{A}{2\pi} k \,, \tag{14}$$

where A is the area of the billiard. The second term is heavily oscillating with k. The sum runs over all periodic orbits including repetitions. l_n is the length of the orbit, and A_n is a factor characterising the stability of the orbit.

The periodic orbit sum (13) divergent, and resummation techniques are needed to calculate the spectrum from the periodic orbits. But the inverse procedure, namely to extract the contributions of the different periodic orbits out of the spectra, is straightforward. For billiards the Fourier transform of the fluctuating part of the density of states,

$$\begin{aligned} \hat{\rho}_{\rm osc}(l) &= \int \rho_{\rm osc}(k) e^{-\imath k l}\, dk \\ &= \sum_n A_n \delta(l - l_n)\,, \end{aligned} \tag{15}$$

directly yields the contributions of the orbits to the spectrum [2]. Each orbit gives rise to a delta peak at an l value corresponding to its length, and a weight corresponding to the stability factor of the orbit.

Figure (11) shows for illustration the squared modulus of the Fourier transform of the spectrum of a microwave resonator shaped as a quarter Sinai billiard [2]. Each peak corresponds to a periodic orbit of the billiard. For the bouncing ball orbit, labelled by ①, three peaks associated with repeated orbits are clearly visible. The smooth part of the density of states is responsible for the increase of $|\hat{\rho}(k)|^2$ at small lengths.

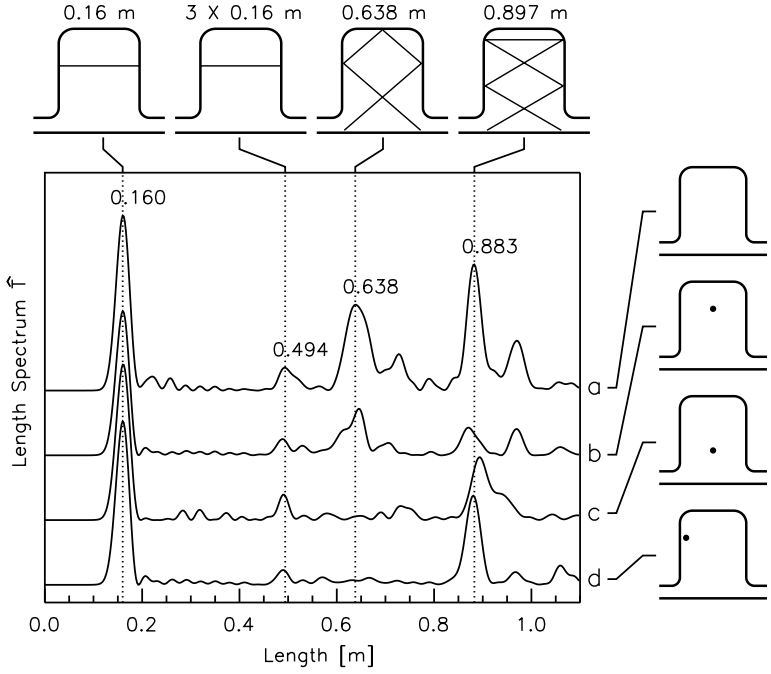

FIGURE 12 – Length spectra $\hat{T} = |\hat{t}|^2$ obtained by a Fourier transformation of the transmission spectrum of a microwave 'quantum dot', for the clean cavity (a), and with the impurity located at three different positions (indicated, b-d). Each maximum in the length spectrum corresponds to a trajectory connecting the entrance with the exit port. Whenever the absorber hits a classical trajectory, the corresponding resonance in the length spectrum is destroyed [25].

In the second example results on the transport through a microwave 'quantum dot', i. e. a resonator with two attached channels, shall be presented. For the transmission amplitude the semiclassical approach yields

$$t(k) = \sum_n A_n e^{ikl_n}\,. \tag{16}$$

The sum is taken over all classical trajectories connecting the input and output channels. l_n now is the length of the nth trajectory with stability factor A_n, and k

is the wavenumber. By taking the Fourier transform of the transmission, one obtains again the stability-weighted length spectrum, allowing for an immediate identification of the relevant transport pathes :

$$\hat{t}(l) = \frac{1}{2\pi} \int t(k) e^{-ikl} dk = \sum_n A_n \delta(l - l_n). \tag{17}$$

In Fig. 12, length spectra $\hat{T} = |\hat{t}|^2$, such obtained are presented. For the empty the cavity (a), the length spectrum shows a number of peaks which can be associated with classical trajectories, shown in the upper part of the figure. With an absorber placed in the cavity, the magnitude of the length peaks depends sensitively on the absorber position position : whenever the absorber lies close to the semiclassical trajectory associated with a particular resonance in the length spectrum, the resonance is destroyed. If, on the other hand, the absorber misses the trajectory, the resonance remains intact. With this technique the length peaks can be associated unambiguously with the corresponding trajectories.

Semiclassical quantum mechanics relates the spectrum to the classical periodic orbits of the system, i. e. to *individual* system properties. In view of this fact one may wonder where the *universal* features discussed in Section 3 come in. To answer this question let us have a look onto the spectral form factor $K(t)$, introduced in Section 3 as the Fourier transform of the spectral autocorrelation function. Entering here with the trace formula, a semiclassical expression for $K(t)$ is obtained, which for billiards read

$$K(t) = \sum_{n,m} A_n^* A_m \delta\left[t - (t_n + t_m)/2\right] e^{\imath k (l_n - l_m) t}. \tag{18}$$

$K(t)$ shows peaks at times $(t_n + t_m)/2$, where $t_n = l_n/c$ is the period for the nth orbit. For short times all these peaks are well-separated. It is essentially this what is seen in Fig. 11. But with increasing time, because of the exponential proliferation of the long orbits in chaotic systems, the density of these peaks becomes so large that only an overall increase of $K(t)$ can be observed. This is the onset of the universal regime. In the so-called diagonal approximation it is argued that only terms with $n = m$ contribute, since the off-diagonal contributions are averaged out by the phase factor $e^{\imath k (l_n - l_m) t}$. For systems with time-reversal symmetry one has to consider in addition that all orbits come in pairs corresponding to clock- and counter-clock-wise propagation. Under this assumption Eq. (18) yields $K_{\mathrm{GOE}} = 2t$ and $K_{\mathrm{GUE}} = t$ being just the leading terms of the expressions given in Eq. (6) for $t < 1$. This had been shown already 30 years ago by M. Berry [26]. It needed 25 more years until it was recognised by M. Sieber and K. Richter [27] that there are off-diagonal terms giving non-negligible contributions. They are associated with pairs of orbits of the topology of the digit '8', one of them self-intersecting, the other one with an avoided crossing instead. The corresponding off-diagonal contributions give the next term in the series expansion of $K(t)$. For the GUE this contribution is zero since here the first order contribution gives already the exact result (as long as $t < 1$). The program was completed by the Haake group [28] who showed that all orders in the expansion can be recovered by considering bundles of orbits with more and more crossings and avoided crossings. In a final step they achieved to extend the validity of the approach to times $t > 1$ [29]. This may be considered as the proof of the BGS conjecture, at least on the level of the spectral form factor.

7 Applications

Occasionally people doubt whether chaotic systems really need an extra quantum-mechanical treatment. The Schrödinger equation after all gives exact results both for

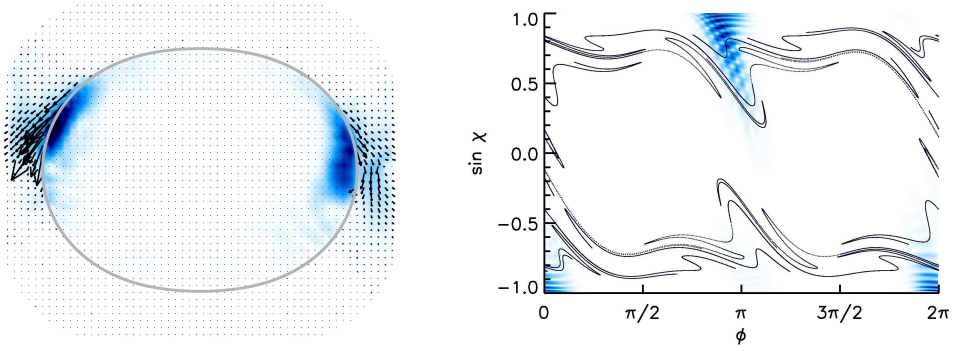

FIGURE 13 – Snapshot of the pulse propagation in a dielectric quadrupole cavity made of teflon (length of the long axis $l = 113\,\mathrm{mm}$). The left figure shows the pulse intensity inside the teflon at the moment of strongest emission in a colour plot. In addition the Poynting vector is shown in the region outside of the teflon. The right figure shows the Husimi distribution of the pulse in a Poincaré plot. In addition the unstable manifold of the rectangular orbit is shown [30].

regular and chaotic systems. Random matrix theory and the random-plane-wave approach, on the other hand mean caricatures of the true situation, and the semiclassical approach at best gives approximate results for high energies. Nowadays the numerical solution of the Schrödinger equation is no challenge any longer even for fairly complicated systems. Why should one resort to old-fashioned techniques which had been abandoned already 80 years ago, after the development of 'correct' quantum mechanics had been been completed ?

First, the semiclassical methods had not been developed as an alternative to the Schrödinger equation to calculate spectra of chaotic systems. This had been successful in exceptional cases only. And random matrix theory had been devised from the very beginning as a tool to understand the universal features of the spectra, but obviously not to get any information on the individual properties.

But the numerical solution of the Schrödinger equation means a black-box calculation, and the human brain is not adopted to perform fast Fourier transforms. This is why spectra as the one shown in Fig. 3 seemingly do not contain any relevant information. But the brain is extremely good in identifying pathes and trajectories, and therefore the representation of the spectra in terms of classical trajectories, as shown in Figs. 11 and Fig. 12 allows an immediate suggestive interpretation.

All this is not just *l'art pour l'art*, as shall be demonstrated by two recent examples.

The relation between wave propagation and classical trajectories had become of practical importance in the development of microlasers. It had been found by Gmachl et al. [31] in quadrupolarly deformed dielectric disks that the strongest emission does not occurs at the points of largest curvature. J. Nöckel an d D. Stone [32] proposed the classical phase space properties to be responsible for this at first sight counterintuitive behaviour. Again this shall be demonstrated by a microwave study. The left part of Fig. 13 shows the snapshot of the pulse propagation in a dielectric quadrupole resonator made of teflon. The pulse had been generated by a Fourier transform from the experimentally determined scattering matrix $S_{12}(\vec{r}_1, \vec{r}_2, k)$, with $\vec{r}_1$ fixed, and $\vec{r}_2$ variable, as described in Section 3. The pulse starts as an outgoing circular wave from an antenna close to the boundary in the lower part of the cavity, but already after a short time only two pulses survive circulating clock- and counter-clockwise close to the border. For the figure a moment has been selected where there is a particularly

strong emission to the outside. In the right part of the figure the same situation is shown in a Poincaré plot, with the polar angle as the abscissa, and the sine of the incidence angle as the ordinate. In a Poincaré plot each trajectory is mapped onto a sequence of points representing the reflections at the boundary. The intricate tongue-like structure represents the instable manifold of the rectangle. It had been obtained by starting a trajectory with a minute deviation from the instable rectangular periodic orbit. In addition the Husimi representation of the pulse in the right hand part of the figure is shown. A Husimi distribution maybe looked upon as a decomposition od a quantum-mechanical wave function in terms of wave packets of minimum uncertainty, and is a convenient tool to establish a correspondence between wave propagation and classical trajectories (see e. g. Ref. [33]). Now it becomes obvious why the strongest emission does *not* occur at the points of strongest emission. Teflon has an index of refraction of $n = 1.44$ meaning a $\sin \chi_{\mathrm{crit}} = 0.69$ for the critical angle of total reflection. Thus the circulating pulses are trapped by total reflection, apart from a weak tunnelling escape due the curvature of the boundary. But whenever the critical line of total reflection is surpassed, there is a strong escape. This happens exactly in the region of the most pronounced tongues of the instable manifold of the rectangular orbit. It is thus this orbit, acting as a dynamical barrier, which is responsible for the observed emission behaviour [34]. In the following years 'phase space engineering' has become an important tool towards the ultimate goal to construct a microcavity with unidirectional emission [35].

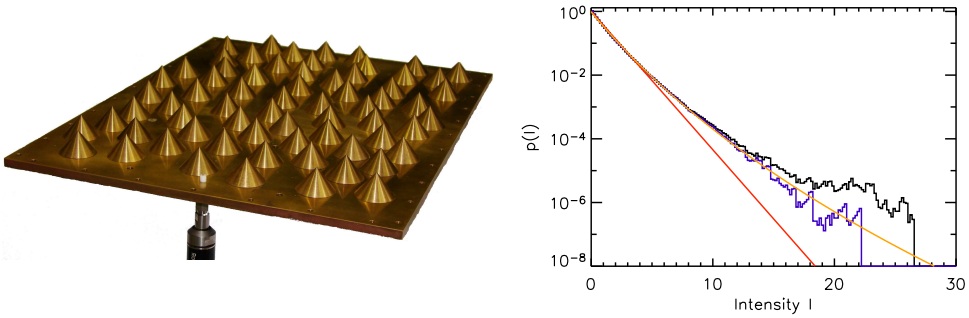

FIGURE 14 – Experimental set-up for the freak wave study (left). The platform has a width of 260 mm, and a length of 360 mm. The source antenna is mounted in the bottom plate close to the border in the centre of the short side. The probe antenna is fixed in the top plate (not shown) and can be scanned in two horizontal dimensions to map the field distribution within the scattering arrangement. The right figure shows the probability distribution of intensities (black). If hot spot regions are excluded from the histogram, the found distribution is in accordance with multi-scattering theory, plotted in orange (light gray). The red (dark gray) line corresponds to the Rayleigh distribution [36].

Another application was motivated by still poorly understood features in the propagation of ocean waves. It had been known for many years that the random plane waves model underestimates the probability for very high amplitudes, called freak or monster waves, by orders of magnitude. Usually non-linearities are blamed for these findings, but it had been found in a recent microwave study [36] that already in the linear regime there are strong deviations from the simple model. The left hand part of Fig. 14 shows the used set-up. Microwaves are propagating through an arrangement of randomly distributed cones acting as scatterers. The right hand part of the figure shows the found intensity distribution. From the random plane wave approach one would expect a distribution according to $p(I) \sim \exp(-I/\langle I \rangle)$, known as Rayleigh's

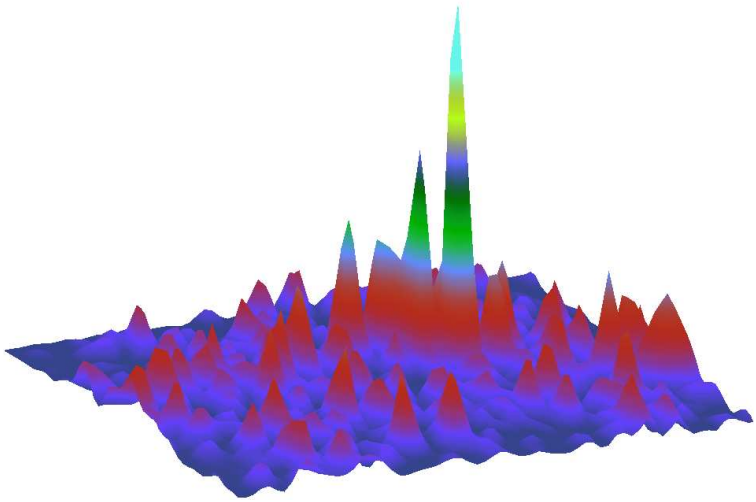

FIGURE 15 – A 'hot spot', observed at a frequency of 8.85 GHz. The experimental probability density for observing such a hot spot is one to two orders of magnitude larger than that expected from multiple scattering theory [36].

law. The actually found probability densities for high intensities are larger by orders of magnitudes. First, there is a multiple scattering correction, which had been known already for some time [37]. But in addition there is another contribution which could be attributed to the formation of hot spots due to caustics in the potential landscape generated by the cones. Figure 15 shows one of these hot spots. Without calling into question the importance of non-linearities for the generation of freak waves in principle, a better understanding of non-random features the linear regime is obviously needed.

The number of activities on the transport of different types of waves, light, seismic waves, water waves, sound waves etc. through disordered media is steadily increasing, many of them based on theories and techniques originally developed in wave and quantum chaos. After several decades of basic research the time for applications has come.

Most of the experimental examples presented in this article have been performed in the author's group at the university of Marburg. I want to thank all my coworkers for their excellent work. In particular I would like to mention my senior coworker U. Kuhl who shared the responsibility for the experiments with me over many years. The experiments had been funded by the Deutsche Forschungsgemeinschaft by numerous individual grants, and during the last three year via the research group 760 "Scattering systems with complex dynamics".

Références

[1] F. Haake, *Quantum Signatures of Chaos. 2nd edition* (Springer, Berlin, 2001).

[2] H.-J. Stöckmann and J. Stein, Phys. Rev. Lett. **64**, 2215 (1990).

[3] H.-J. Stöckmann, *Quantum Chaos - An Introduction* (University Press, Cambridge, 1999).

[4] M. C. Gutzwiller, *Chaos in Classical and Quantum Mechanics, Interdisciplinary Applied Mathematics, Vol. 1* (Springer, New York, 1990).

[5] D. Ullmann, Eur. Phys. J. Special Topics **145**, 25 (2007).

[6] H.-J. Stöckmann, Eur. Phys. J. Special Topics **145**, 15 (2007).

[7] F. Melde, *Chladnis's Leben und Wirken* (N. G. Elwert'sche Verlagsbuchhandlung, Marburg, 1888).

[8] U. Kuhl, H.-J. Stöckmann, and R. Weaver, J. Phys. A **38**, 10433 (2005).

[9] J. Stein and H.-J. Stöckmann, Phys. Rev. Lett. **68**, 2867 (1992).

[10] E. J. Heller, Phys. Rev. Lett. **53**, 1515 (1984).

[11] J. Stein, H.-J. Stöckmann, and U. Stoffregen, Phys. Rev. Lett. **75**, 53 (1995).

[12] M. L. Mehta, *Random Matrices. 2nd edition* (Academic Press, San Diego, 1991).

[13] M. R. Zirnbauer, J. Math. Phys. **37**, 4986 (1996).

[14] O. Bohigas, M. J. Giannoni, and C. Schmit, Phys. Rev. Lett. **52**, 1 (1984).

[15] G. Casati, F. Valz-Gris, and I. Guarnieri, Lett. Nuov. Cim. **28**, 279 (1980).

[16] C. W. J. Beenakker, Rev. Mod. Phys. **69**, 731 (1997).

[17] H. Alt *et al.*, Phys. Rev. E **55**, 6674 (1997).

[18] S. W. McDonald and A. N. Kaufman, Phys. Rev. Lett. **42**, 1189 (1979).

[19] K. Schaadt, T. Guhr, C. Ellegaard, and M. Oxborrow, Phys. Rev. E **68**, 036205 (2003).

[20] V. Doya, O. Legrand, F. Mortessagne, and C. Miniatura, Phys. Rev. Lett. **88**, 014102 (2002).

[21] M. V. Berry, J. Phys. A **10**, 2083 (1977).

[22] S. Hortikar and M. Srednicki, Phys. Rev. Lett. **80**, 1646 (1998).

[23] U. Dörr, H.-J. Stöckmann, M. Barth, and U. Kuhl, Phys. Rev. Lett. **80**, 1030 (1998).

[24] A. Einstein, Verhandlungen der Deutschen Physikalischen Gesellschaft **19**, 82 (1917).

[25] Y.-H. Kim *et al.*, Phys. Rev. B **68**, 045315 (2003).

[26] M. V. Berry, Proc. R. Soc. Lond. A **400**, 229 (1985).

[27] M. Sieber and K. Richter, Phys. Scr. **T90**, 128 (2001).

[28] S. Müller *et al.*, Phys. Rev. Lett. **93**, 014103 (2004).

[29] S. Heusler *et al.*, Phys. Rev. Lett. **98**, 044103 (2007).

[30] R. Schäfer, U. Kuhl, and H.-J. Stöckmann, New J. of Physics **8**, 46 (2006).

[31] C. Gmachl *et al.*, Science **280**, 1556 (1998).

[32] J. U. Nöckel and A. D. Stone, Nature **385**, 45 (1997).

[33] A. Bäcker, S. Fürstberger, and R. Schubert, Phys. Rev. E **70**, 036204 (2004).

[34] H. G. L. Schwefel *et al.*, J. Opt. Soc. Am. B **21**, 923 (2004).

[35] J. Wiersig and M. Hentschel, Phys. Rev. Lett. **100**, 033901 (2008).

[36] R. Höhmann *et al.*, Phys. Rev. Lett. **104**, 093901 (2010).

[37] T. M. Nieuwenhuizen and M. C. W. van Rossum, Phys. Rev. Lett. **74**, 2674 (1995).